

Effect of temperature variations and thermal noise on the static and dynamic behavior of straintronics devices

Mahmood Barangi and Pinaki Mazumder

Citation: *J. Appl. Phys.* **118**, 173902 (2015); doi: 10.1063/1.4934566

View online: <http://dx.doi.org/10.1063/1.4934566>

View Table of Contents: <http://aip.scitation.org/toc/jap/118/17>

Published by the [American Institute of Physics](#)

Effect of temperature variations and thermal noise on the static and dynamic behavior of straintronics devices

Mahmood Barangi^{a)} and Pinaki Mazumder

Department of Electrical Engineering and Computer Science, University of Michigan, Ann Arbor, Michigan 48109, USA

(Received 25 May 2015; accepted 13 October 2015; published online 4 November 2015)

A theoretical model quantifying the effect of temperature variations on the magnetic properties and static and dynamic behavior of the straintronics magnetic tunneling junction is presented. Four common magnetostrictive materials (Nickel, Cobalt, Terfenol-D, and Galfenol) are analyzed to determine their temperature sensitivity and to provide a comprehensive database for different applications. The variations of magnetic anisotropies are studied in detail for temperature levels up to the Curie temperature. The energy barrier of the free layer and the critical voltage required for flipping the magnetization vector are inspected as important metrics that dominate the energy requirements and noise immunity when the device is incorporated into large systems. To study the dynamic thermal noise, the effect of the Langevin thermal field on the free layer's magnetization vector is incorporated into the Landau-Lifshitz-Gilbert equation. The switching energy, flipping delay, write, and hold error probabilities are studied, which are important metrics for nonvolatile memories, an important application of the straintronics magnetic tunneling junctions. © 2015 AIP Publishing LLC. [<http://dx.doi.org/10.1063/1.4934566>]

I. INTRODUCTION

The discovery of tunnel magnetoresistance (TMR) in magnetic tunneling junction (MTJ)¹ was followed by a plethora of theoretical and practical studies in research labs to develop a new generation of nonvolatile magnetic memories, called magnetic random access memories (MRAM).²⁻⁴ However, in the early stages, industry did not warmly welcome MRAM, as the proposed methods for writing into the magnetic cell were energy hungry and area inefficient, failing to compete with charge-based memories at the time. Field induced magnetization switching (FIMS),² as the first proposed method for writing data into MTJ, relied on the magnetic field generated by the current flow in a neighboring wire. High requirements of static current in order to generate a strong magnetic field and the possibility of half-select errors were the main shortcomings of this method. The discovery of spin transfer torque (STT) for MTJ switching,⁵ which relies on spin-polarized currents, revitalized MRAM research and development.⁶⁻¹⁰ STT is a much more energy efficient method than FIMS and is scalable with the complementary metal-oxide-semiconductor (CMOS) integrated circuits (IC).^{11,12}

Both FIMS and STT, however, employ a flow of static current to achieve magnetization vector switching in the free layer of the MTJ. The use of static charge flow essentially nullifies the inherent energy advantage of the magnetic logic ($E_{\text{min-charge}} = N \times E_{\text{min-magnetic}}$, N being the number of charge carriers, and $E_{\text{min-charge}}$ and $E_{\text{min-magnetic}}$ being the minimum energy required to switch the state of a charge-based logic and magnetic logic, respectively¹³). In order to maximize the energy efficiency, the amount of charge

employed for MTJ switching should be minimized. To this end, the recently-proposed straintronics principle, a combination of piezoelectricity and magnetostriction, is an alternative approach that overcomes the aforementioned obstacle.¹⁴⁻¹⁸ The amount of charge consumed for switching the MTJ's state in straintronics is well below STT and FIMS.^{15,16}

Temperature variations can severely impact both static and dynamic responses of straintronics devices. The former is affected due to the strong dependency of the saturation magnetization, shape anisotropy, magnetocrystalline anisotropy, and magnetostriction coefficient on temperature.¹⁹⁻²² While these parameters assume a fairly fixed value at low temperatures, when approaching the Curie temperature, T_C , they fall dramatically, bringing the free layer close to a paramagnetic state. The energy barrier (EB) and, as a result, the critical flipping voltage of the free layer in the straintronics device, are strong functions of temperature. It is specifically worthwhile to investigate the variations of the above parameters at temperature ranges between 200 K and 400 K, as this is the operating range of a wide variety of integrated circuits.²³

The dependency of the device's dynamic response is realized by incorporating the Langevin thermal noise field, representing the thermal noise, into the Landau-Lifshitz-Gilbert (LLG) equation. The random noise field has three important impacts on the dynamic behavior: (i) it assists with the magnetization vector's flipping—without it, the magnetization will stagnate at relaxation state and will not respond to the applied stress;¹⁶ (ii) a larger thermal noise leads to larger fluctuations of the magnetization vector, resulting in a faster response and reducing the write error probability (WEP); and (iii) fluctuations can also lead to hold error probabilities (HEP), also known as retention

^{a)}Email: barangi@umich.edu

errors, which are hazardous to straintronics-based MRAM design.

Due to its crucial importance, the effect of thermal noise on the dynamic behavior of the magnetization in a nanomagnet has been the subject of study in the literature.^{24–27} A general study of the dynamics in a single domain magnet under Langevin thermal noise has been published previously,²⁴ providing a comprehensive statistical analysis on the magnetization dynamics with and without the effect of external magnetic field. Analysis of the dynamics in strain-induced multiferroics has also been the subject of study recently.^{25–27} These works mainly focus on the effect of dynamic thermal noise on the switching behavior of a single magnet under stress and investigate the switching reliability under different stress removal conditions. While the study of the thermal noise is of significant importance, a comprehensive model that investigates the effect of temperature fluctuations and thermal noise on both static and dynamic behaviors of the straintronics device has yet to exist.

In this paper, we perform an in-depth analysis on the temperature dependency of the static and dynamic metrics of the straintronics MTJ. In search for the proper material for straintronics-based integrated circuits, we investigate four common magnetostrictive materials. The effect of the Langevin thermal field on the initial magnetization angle and the delay metrics of the straintronics device, and the resulting WEP and HEP are studied in detail. The flipping energy and the energy-delay trade-off for the straintronics-based system design are analyzed. The rest of the paper is organized as follows: Section II introduces the device architecture and the principle of operation; Section III introduces the dependency of the magnetic anisotropies on temperature; Section IV analyzes the energy barrier and the critical voltage and their variations with temperature; Section V introduces the Langevin field and its effect on the magnetization vector's dynamic response; Section VI presents WEP, HEP, and energy-delay trade-off as important metrics for memory design; and Section VII concludes the paper.

II. THE STRAINTRONICS DEVICE

Strain-assisted switching and details of read and write operations of the device are studied in detail in previous works.^{15,16,28} In this section, a brief introduction of the device's architecture and the switching principle is provided. The architecture of the straintronics MTJ is given in Fig. 1(a). The device is made by placing a piezoelectric layer (PZT) on top of the magnetostrictive free layer of an MTJ. The device is shaped as a rectangle with the major and minor axes lying along the z -axis and y -axis, respectively, as demonstrated in Fig. 1(a). The PZT is modeled as a parallel plate capacitance, and the MTJ is a variable resistor. The resistance of the MTJ is a function of the relative orientation of the free layer's magnetization vector compared to the magnetization of the pinned layer. The resistance assumes its minimum and maximum in parallel and antiparallel orientations, respectively. The state of the MTJ can be read via sensing the resistance level by sending a small current through the free layer into the MTJ.²⁹ The PZT interface occupies most of the free layer

to assure efficient transfer of the strain.²⁹ In this paper, a complete transfer of strain is assumed between the PZT and the free layer. A shift in the critical switching voltage of the straintronics device may result in the case of partial strain transfer. Nevertheless, such a shift will not affect the thermal analysis procedure used in this paper. The thickness of the free layer is chosen to be 10 nm and the major and minor axes are 120 nm and 80 nm, respectively.

In the absence of an external stress, the intrinsic magnetic energy of the free layer creates an EB between parallel ($\theta = 0$) and antiparallel ($\theta = \pi$) orientations as demonstrated in Fig. 1(a). Therefore, the magnetization vector prefers to stay along the major axis. An applied voltage across the straintronics device creates a strain in the PZT, which will be transferred to the free layer of the MTJ. The stress in the magnetostrictive free layer will reduce the magnetic energy barrier. A higher stress level can eliminate the energy barrier, forcing the magnetization vector to rotate and settle along the minor axis ($\theta = \pi/2$) as demonstrated in Fig. 1(b). Switching the state of the magnetization vector from the major axis to the minor axis, denoted as the write event, is, therefore, possible by applying a voltage across the device. This is the principle of straintronics magnetization switching. The use of voltage instead of current brings major energy savings to the table. This energy efficiency, however, comes at the expense of more complicated write algorithms and iterative methods in memory applications.²⁸ The latter is because a write operation in MTJ-based memories consists of flipping of the magnetization from parallel to antiparallel orientation or vice versa, which is warranted in STT-based switching, but requires iterative methods in straintronics memories.²⁸ Nevertheless, the straintronics method still demonstrates remarkable advantages over STT switching when it comes to energy-delay products²⁹ (a metric to evaluate the tradeoff between energy and delay), making it a promising candidate for future memory applications.

The static metrics of the discussed device, including the intrinsic and stress anisotropy energies, the energy barrier, and the critical voltage required for switching, are strong functions of temperature, which will be comprehensively discussed Sections III and IV.

III. DEPENDENCY OF STATIC BEHAVIOR ON TEMPERATURE

The magnetic energy of the straintronics device has three major components:¹⁵ (i) shape anisotropy (E_{sh}), which is the tendency of the magnetization vector to settle along a certain direction due to the shape of the free layer; (ii) uniaxial anisotropy (E_u), also called magnetocrystalline anisotropy, which is primarily due to the spin-orbit interactions, and magnetizes the free layer in a certain direction; and (iii) stress anisotropy (E_σ), which is due to the applied stress across the magnetostrictive free layer. Hence, the total magnetic energy, E_{mag} , of the free layer can be expressed as¹⁵

$$E_{mag} = E_{sh} + E_u + E_\sigma, \quad (1)$$

where

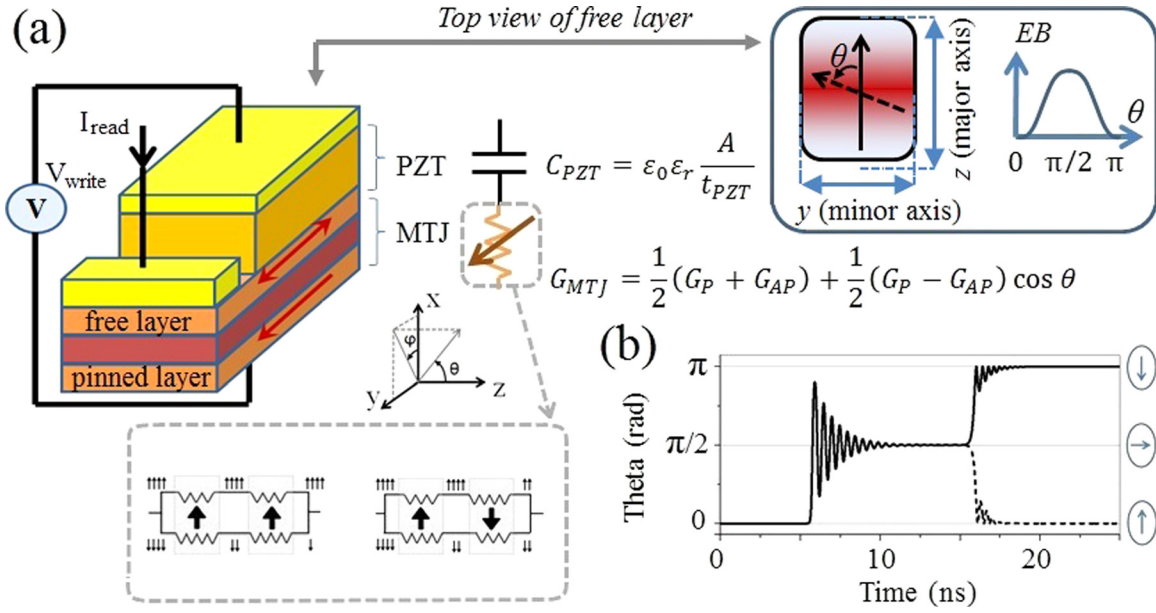


FIG. 1. (a) View of the straintronics device and the demonstration of the equivalent electrical model, G_P and G_{AP} are the conductances of the MTJ in parallel and antiparallel orientations; the resistance of the MTJ, R_{MTJ} is simply obtained as $R_{MTJ} = 1/G_{MTJ}$, (b) dynamic flipping of the magnetization vector under stress; the magnetization rotates and settles along the minor axis when the stress is retained between 5 ns and 15 ns.

$$E_{sh} = \frac{\mu_0}{2} M_s^2 N_{sh} V, \quad (2)$$

$$E_u = K_u V \sin^2 \theta, \quad (3)$$

$$E_\sigma = \frac{3}{2} \lambda_s \sigma V \sin^2 \theta_\sigma. \quad (4)$$

In the above equations, μ_0 is the permeability of vacuum, M_s is the saturation magnetization, N_{sh} is the demagnetization factor, K_u is the uniaxial anisotropy coefficient, λ_s is the magnetostrictive expansion at saturation, σ is the applied stress, V is the free layer's volume, and θ_σ is the angle of the magnetization vector with the minor axis. It should be noted that combining shape and uniaxial anisotropy energies gives intrinsic magnetic energy to the free layer, while the stress anisotropy is the external magnetostrictive force that switches the state of the free layer using the straintronics principle.

In order to study the static metrics of the straintronics device, the variations in the magnetic parameters and energy levels should be examined.³⁰ Modeling the effect of temperature on the saturation magnetization of the free layer is analyzed in the supplementary material.³¹ Next, we will inspect the temperature dependency of different terms in the total magnetic energy of the straintronics device. In this work, the downfall of exchange interactions at temperatures close to Curie temperature is not accounted for. The latter can compromise the single domain assumption of the nanomagnet at temperatures around T_C and should be handled with care whenever necessary.

A. Shape anisotropy

Shape anisotropy, as formulated in (2), is one of the major decision makers of the free layer's energy barrier. From (2), the variations in M_s^2 with temperature can be

predicted using the Brillouin function.³¹ However, the variations of N_{sh} and V due to thermal expansion should also be further investigated.

The demagnetization factor, $N_{sh} = N_{zz} \cos^2 \theta + N_{yy} \sin^2 \theta \sin^2 \varphi + N_{xx} \sin^2 \theta \cos^2 \varphi$, for the device in Fig. 1, assumes its maximum along the x -axis and its minimum along the y -axis. The parameters N_{xx} , N_{yy} , and N_{zz} are obtained using the following equations:¹⁵

$$N_{zz} = \frac{\pi t}{4a} \left(1 - \frac{1}{4} \left(\frac{a-b}{a} \right) - \frac{3}{16} \left(\frac{a-b}{a} \right)^2 \right), \quad (5)$$

$$N_{yy} = \frac{\pi t}{4a} \left(1 + \frac{5}{4} \left(\frac{a-b}{a} \right) + \frac{21}{16} \left(\frac{a-b}{a} \right)^2 \right), \quad (6)$$

$$N_{xx} = 1 - (N_{yy} + N_{zz}), \quad (7)$$

where a , b , and t are the free layer's major axis, minor axis, and thickness, respectively. Variations in temperature, T , will lead to compression or expansion. However, the relative ratios of t/a and $(a-b)/a$, which are decision makers in (5) and (6), will stay constant, assuming a linear thermal expansion ($\Delta L/L = \alpha_L \Delta T$, α_L being the material's expansion coefficient, L and ΔL being the length and change in length, respectively, and ΔT being the temperature variations).

Lastly, due to the small value of α_L , the variations in volume due to thermal expansion are negligible compared to the changes in $M_s(T)$. For example, Nickel exhibits merely 0.4% increase in its volume for every 100° increase in temperature.

As a result of the above discussion, the shape anisotropy's dependency on temperature can be summarized as

$$\frac{E_{sh}(T)}{E_{sh0}} = \left(\frac{M_s(T)}{M_{s0}} \right)^2, \quad (8)$$

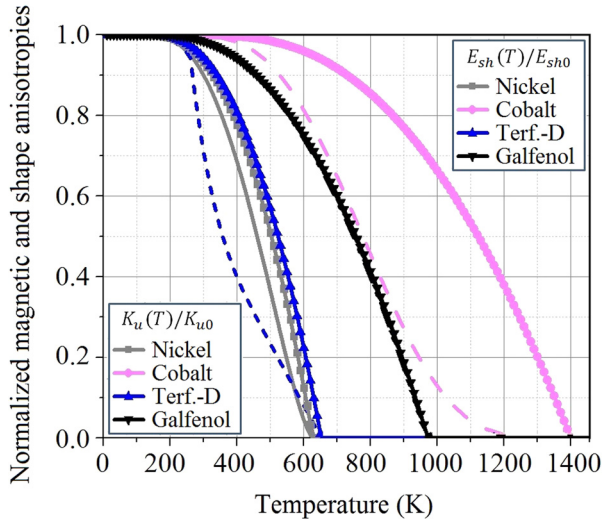


FIG. 2. The dependency of shape and uniaxial anisotropies on temperature up to the Curie levels for different materials; as the Curie temperature is reached, the materials lose their intrinsic magnetic energies and approach a paramagnetic state.

where E_{sh0} is the value of shape anisotropy at near-zero temperatures.

B. Magnetocrystalline anisotropy

According to Callen and Callen's theory,³² the dependence of the uniaxial anisotropy constant on temperature originates from the changes in $M_s(T)$, and can be expressed as³²

$$\frac{K_u(T)}{K_{u0}} = \left(\frac{M_s(T)}{M_{s0}} \right)^m, \quad (9)$$

where K_{u0} is the uniaxial anisotropy's constant near absolute zero temperature. For cubic and uniaxial crystals, $m = 3$ and $m = 10$, respectively.³³ Therefore, Nickel and Cobalt will have the powers of 3 and 10 in the above equation, respectively.

Although Callen and Callen's theory predicts the temperature dependency of the magnetocrystalline anisotropy fairly well for pure element crystals, it is shown that it fails to predict the temperature dependency of K_u for alloys.³³ Hence, the variations in the uniaxial coefficient for Galfenol and Terfenol-D should be investigated separately.

Given the crystal structure of Galfenol ($Fe_{1-x}Ga_x$, $0.13 \leq x \leq 0.24$), using the power $m = 2.1$ provides a fairly accurate estimation.³⁴⁻³⁷ Terfenol-D ($(Tb, Dy)Fe_2$), however, is

considered as a rare-earth 3d-transition-metal alloy. For these alloys, the magnetic anisotropy transits through three different phases:^{38,39}

- (i) When the temperature of the alloy is below the spin reorientation temperature, T_{SR} , the magnetic anisotropy follows the famous power law in (9), in which $m = l(l + n - 2)/(n - 1)$. For lowest order anisotropy $l = 2$, and assuming a planar model in which $n = 2$, we will have $m = 4$. The value of T_{SR} for Terfenol-D is $\sim -10^\circ\text{C}$,^{39,40} which means that, up to this temperature, the power law is enforced.
- (ii) For the values above spin-reorientation temperature, the behavior is mostly dominated by the rare-earth elements and is given by³⁸

$$\frac{K_u(T)}{K_{u0}} = \frac{J_{SR}^2}{n(n+2)k^2T^2}, \quad (10)$$

where k is the Boltzmann constant and J_{SR} is an alloy-dependent constant and can be obtained by assuming a continuous transition of $K_u(T)$ at the spin reorientation temperature.

- (iii) When the temperature approaches the Curie temperature, (10) fails to predict the behavior. The behavior, at this point, can be expressed as³⁸

$$\frac{K_u(T)}{K_{u0}} = 1 - \frac{T}{T_C}. \quad (11)$$

By combining the three regions above, the uniaxial anisotropy of Terfenol-D can be predicted. Our simulations on the magnetic anisotropy of Terfenol-D closely follow reports in the literature.^{40,41}

Fig. 2 contains the simulation data on the normalized variations of shape and uniaxial anisotropies, as the temperature increases for four materials. The values are also re-plotted for a 200 K–400 K IC temperature range in Fig. 3, and the percentages of anisotropy reduction for the four materials along with their magnetic properties^{16,42-47} used in our simulation model are listed in Table I. Dramatic reductions of both shape anisotropy and uniaxial anisotropy reveal the critical influence of temperature on the device's energy barrier, an important metric for non-volatile memory design.

C. Magnetostriction expansion at saturation

The magnetostriction expansion at saturation, λ_s , plays a major role in determining the critical stress required for

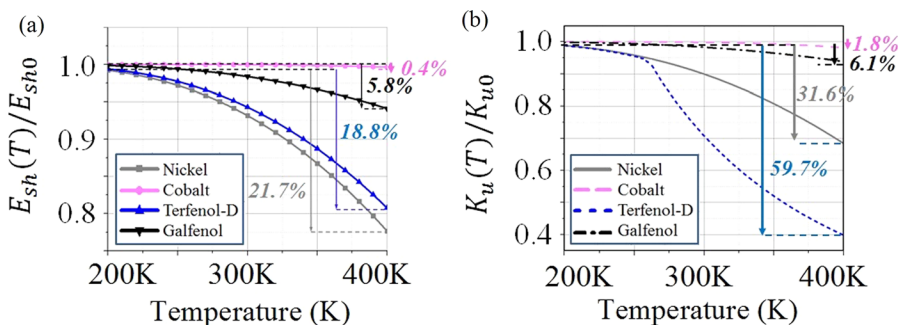


FIG. 3. Further demonstration of the (a) shape and (b) uniaxial anisotropies' variations within 200 K and 400 K.

TABLE I. Materials' properties and the percentage of reduction in shape, uniaxial, and stress energies of different magnetostrictive materials when the temperature is raised from 200 K to 400 K.

	Nickel	Cobalt	Terfenol-D	Galfenol
M_s (kA/m)	510	1400	912	1340
K_u (kJ/m ³)	12	16	1.6	5
$ \lambda_s $ (ppm)	20	20	600	200
T_C (K)	627	1400	652	972
E_{sh} (%)	21.7	0.4	18.8	5.8
E_u (%)	31.6	1.8	59.7	6.1
E_σ (%)	30.8	0.6	26.6	8.2

flipping the magnetization state of the straintronics device. The dependency of this parameter on temperature is expressed using the reduced hyperbolic Bessel function^{48,49}

$$\frac{\lambda_s(T)}{\lambda_{s0}} = \hat{I}_{\frac{3}{2}}(u), \quad (12)$$

where $\coth(u) - 1/u = M_s(T)/M_{s0}$. The simulation results are plotted in Fig. 4 for the four magnetostrictive materials. The simulation results are in fair accordance with the reported behavior in the literature.^{21,48-51} In fact, it is demonstrated that the hyperbolic Bessel function in molecular-field approximation holds accurately at all temperatures up to Curie temperature,³² while at low temperatures, the magnetostriction coefficient follows the same power laws as magnetic anisotropy. The percentages of variations in E_σ due to λ_s variations, when the temperature rises from 200 K to 400 K, are tabulated in Table I for the sake of comparing different materials.

From the obtained metrics in Table I, it is understood that Cobalt and Galfenol show the least amount of variation in the temperature range of interest, while Nickel and Terfenol-D show dramatic variations in their magnetic parameters. This is mainly due to the high Curie temperature of Cobalt and Galfenol, which might make them the preferred candidates to be integrated into electronic circuits. Terfenol-D, although demonstrating fast response and low switching

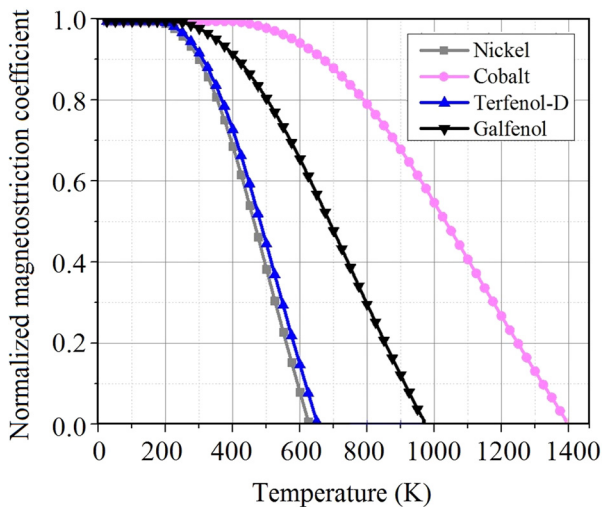


FIG. 4. The dependency of the magnetostriction coefficient on temperature as predicted by the hyperbolic Bessel function.

voltage,^{15,16} is not an ideal candidate for temperature-sensitive straintronics-based integrated circuits, as its magnetic properties vary dramatically with temperature variations, a phenomenon that frequently occurs in circuit chips.

IV. ENERGY BARRIER AND CRITICAL FLIPPING VOLTAGE

The energy barrier of the device, arising from its intrinsic shape and uniaxial anisotropies,¹⁵ is a measure of the device's immunity against the thermal noise and magnetic interferences. Assuming the rotation of the magnetization vector within the y - z plane, which is enforced by shape anisotropy, the energy barrier is defined as $EB = E_{mag}(\theta = \pi/2) - E_{mag}(\theta = 0 \text{ (or } \pi))$. From the discussions in Section III, it is naturally expected that the barrier will reduce as the temperature increases due to the fall in the magnetic anisotropies. This is demonstrated in Fig. 5(a), where the energy barrier is plotted for Nickel as a function of temperature in the absence of stress. A contour map of the energy barrier's graph is re-plotted in Fig. 5(b) to further demonstrate the energy behavior as a function of temperature. From the two graphs, the following conclusions can be drawn: (i) the intrinsic magnetic energy assumes its minimum in the parallel and antiparallel orientation and its maximum when the magnetization is oriented along the minor axis; (ii) the energy barrier reduces and eventually vanishes as the temperature approaches the Curie level, where the material reaches a paramagnetic state; and (iii) the absolute value of the energy at any orientation of the magnetization vector (for example, at $\theta = 0$) also reduces as temperature increases. For example, from Fig. 5(a), at $\theta = 0$, the magnetic energy at near-zero temperature is eliminated as the temperature approaches T_C .

It is particularly worthwhile to investigate the effect of stress and temperature on the device's thermal stability, $\Delta = EB/kT$, which is an important data retention metric in non-volatile memory design. Usually, a thermal stability factor larger than 40 is required for storage class memories.⁵² The thermal stability of the straintronics device, with Galfenol as the magnetostrictive material, is demonstrated as a function of temperature for different stress values in Fig. 6. It is observed that as the temperature merges with T_C , a sharp reduction in the thermal stability is observed. Furthermore, increasing stress reduces the thermal stability linearly, which is expected from (1) and (4). In general, it is observed that Galfenol keeps its thermal stability well above 40, within a 200 K to 400 K temperature range, even at stress values closer to its critical stress ($\sigma_C \approx 180$ MPa for Galfenol in our simulations).

Lastly, the effect of temperature on the minimum voltage required for the magnetization flipping, also called the critical voltage, V_C , should be analyzed. By equating anisotropy energies, it is concluded that

$$V_C = \frac{\left(\frac{\mu_0}{2} M_s^2 (N_{yy} - N_{zz}) + K_u\right) t_{PZT}}{\frac{3}{2} \lambda_s Y d_{31}}, \quad (13)$$

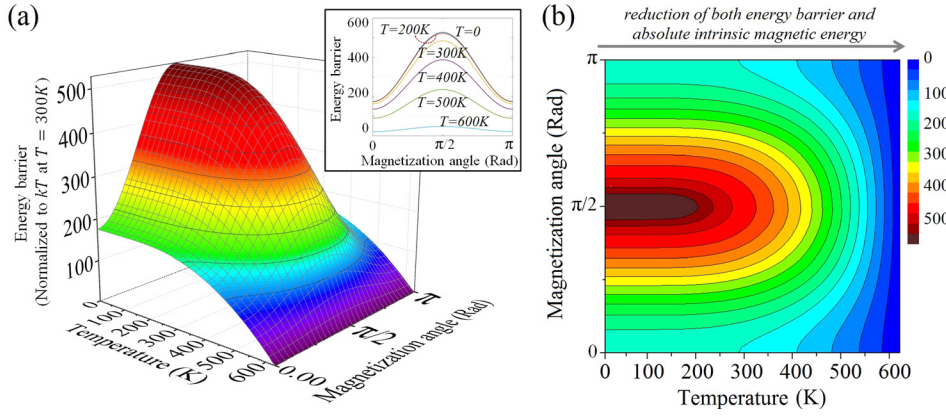


FIG. 5. (a) and (b) The dependency of the energy barrier of Nickel on temperature; as the temperature rises, both the energy barrier and the absolute values of energy are reduced.

where t_{PZT} is the thickness of the PZT, Y is the Young Modulus of the free layer, and d_{31} is PZT's dielectric coefficient. The dependency of V_C on temperature is simulated in Fig. 7 for different magnetostrictive materials. By observing the graphs closely, the critical voltage goes through two different slope phases as the temperature increases. First, at low temperatures, V_C slightly reduces as temperature increases. Then, an increase in the value of the critical voltage is observed at higher temperatures. This behavior can be analyzed by taking the derivative of (13) with respect to temperature

$$\frac{dV_C}{dT} = \frac{A \frac{dM_s}{dT} + B \frac{dK_u}{dT} - C \frac{d\lambda_s}{dT}}{\left(\frac{3}{2} \lambda_s Y d_{31}\right)^2}, \quad (14a)$$

$$A = \frac{3}{2} \lambda_s Y d_{31} \mu_0 (N_{yy} - N_{zz}) M_s t_{PZT}, \quad (14b)$$

$$B = \frac{3}{2} \lambda_s Y d_{31} K_u t_{PZT}, \quad (14c)$$

$$C = \frac{3}{2} Y d_{31} \left(\frac{\mu_0}{2} M_s^2 (N_{yy} - N_{zz}) + K_u \right) t_{PZT}. \quad (14d)$$

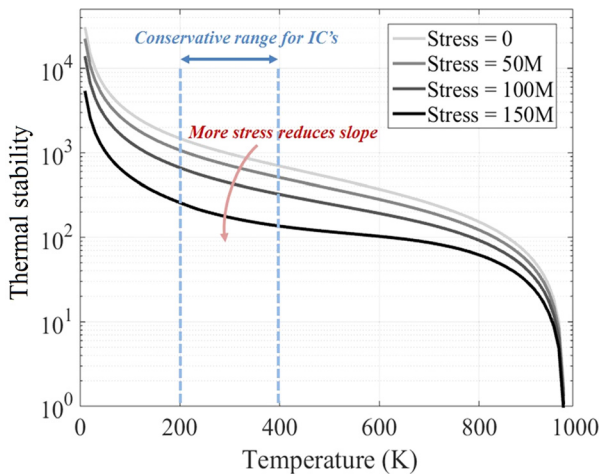


FIG. 6. The dependency of thermal stability of Galfenol on temperature and applied stress; the graph shows two fast regions: (i) at low temperatures, where the parameter kT rises, and (ii) at temperatures close to T_C , where the energy barrier approaches zero.

The saturation magnetization starts degrading at lower temperatures compared to the magnetostriction coefficient. As a result, when $T \ll T_C$, we have $dV_C/dT < 0$, and a slight reduction of the critical voltage is observed. This behavior is more noticeable for Cobalt on the graphs, mainly due to its high M_s and very low λ_s . As the temperature rises, λ_s starts decreasing according to (12), while M_s and K_u continue to fall as predicted by the saturation magnetization's behavior³¹ and (12)–(14), respectively. When the slope of $d\lambda_s/dT$ is large enough to fulfill $A \times dM_s/dT + B \times dK_u/dT - C \times d\lambda_s/dT > 0$, the critical voltage will begin to rise.

From the inset of Fig. 7, it is also concluded that Galfenol and Cobalt keep their critical voltage at a fairly constant level, while Terfenol-D and Nickel show almost 7% and 4% increases in V_C within a 200 K to 400 K temperature range, respectively. This can come in handy when considering a straintronics-based system design for temperature-sensitive applications.

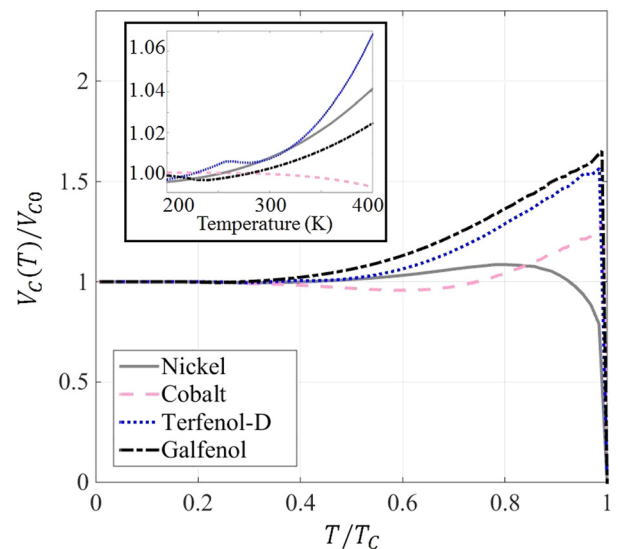


FIG. 7. The dependency of the critical flipping voltage on temperatures up to the Curie levels for four magnetostrictive materials; the variations within 200 K–400 K are demonstrated in the inset of the figure, showing that the four materials maintain an almost-constant critical voltage within the range of interest; the results are normalized to V_{C0} , the critical flipping voltage near absolute zero temperature.

V. DYNAMIC THERMAL NOISE FIELD

The dynamic response of the magnetization vector in a straintronics device is predicted using the LLG equation given by⁵³

$$\frac{d\vec{M}}{dt} = -\frac{\gamma_0}{(1+\alpha^2)}(\vec{M} \times \vec{H}) - \frac{\gamma_0}{M_s \times \left(\alpha + \frac{1}{\alpha}\right)}\vec{M} \times (\vec{M} \times \vec{H}), \quad (15)$$

where M is the magnetization vector, γ_0 is the gyromagnetic ratio, α is the Gilbert damping factor, and $H = H_r\hat{r} + H_\theta\hat{\theta} + H_\phi\hat{\phi}$ is the net magnetic field due to shape and uniaxial anisotropies and the applied stress.¹⁵ The effect of thermal noise is modeled by following the same procedure developed by Brown⁵⁴ and Grinstein.⁵⁵ The thermal flux density can be incorporated in (15) by including the Langevin thermal noise field, H_N , in the total magnetic field; i.e., $H_{tot} = H + H_N$, where H_N is a Gaussian random noise field variable³¹ with a strength of $D = 2kT\alpha/\mu_0\gamma_0M_sV$, and a correlation of

$$\langle H_i(x, t)H_j(x', t') \rangle = D\delta_{ij} \times \delta(x - x')\delta(t - t'). \quad (16)$$

Therefore, the thermal noise field to be incorporated in (15) can be expressed as

$$H_{N,i} = \sqrt{\frac{2\alpha kT}{\mu_0\gamma_0M_sV}}X_i(t) \quad i = (x, y, z), \quad (17)$$

where $X_i(t)$'s are uncorrelated zero-mean unit-variance Gaussian random variables in the direction of Cartesian axes.

The relative ratio of the thermal noise field to the net magnetic field of the device (i.e., H_{N-rms}/H) can be simulated to observe the strength of the thermal noise. It is expected that as we increase the stress level, the net magnetic field forcing the magnetization vector to stay along the easy

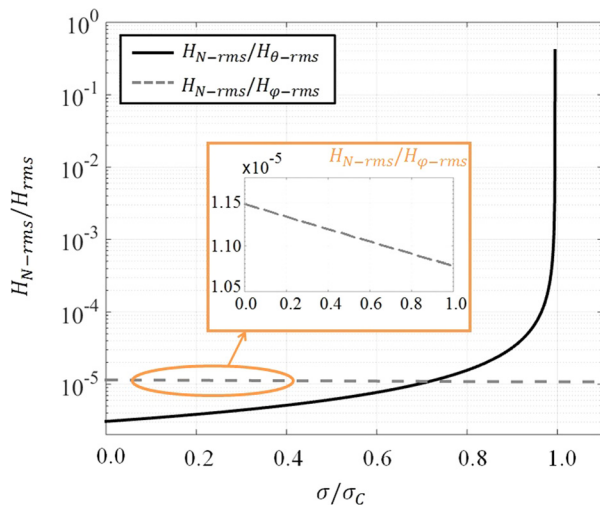


FIG. 8. The effect of stress on the relative strength of the thermal noise; as the stress increases, H_N/H_θ rises, leading to more fluctuations around the z -axis, while H_N/H_ϕ decreases slightly (inset), increasing the magnetization vector's tendency to stay within the y - z plane.

axis (H_θ) becomes weaker.³¹ It is also shown³¹ that as we increase the stress, the value of H_ϕ , which forces the magnetization to stay in plane (within the y - z plane of Fig. 1(a)), increases slightly. Therefore, an increase in stress increases H_{N-rms}/H_θ as demonstrated in Fig. 8, allowing the magnetization to fluctuate more easily around the easy axis. As the stress approaches its critical value, the thermal noise becomes significantly stronger owing to the fact that³¹ $\lim_{\sigma \rightarrow \sigma_c} H_\theta = 0$. It is also observed from Fig. 8 that as we increase the stress, H_{N-rms}/H_ϕ slightly reduces. This means that while the magnetization vector's fluctuations around the major axis (z -axis) increase at higher stress levels, its tendency to stay within the y - z plane increases slightly, leading to more in-plane fluctuations.

The flipping delay of the straintronics device (also called the alignment delay in some works) is a strong function of the initial magnetization angle, θ_i , which is mainly due to the thermally stimulated agitations. It is shown that the initial magnetization angle has a zero-mean Gaussian distribution with the strength of⁵⁶

$$\theta_{i-rms} = \sqrt{\frac{kT}{\mu_0VM_sH}}. \quad (18)$$

Due to the dependency of the flipping delay on the initial magnetization angle, Gaussian fluctuations of θ_i lead to variations in the flipping delay, t_d . This is demonstrated in Fig. 9, where our thermally-incorporated model based on (15)–(17) is simulated at room temperature. The dynamic waveforms of the magnetization flipping for $N = 200$ samples and the resulting histogram for the flipping delays are demonstrated. The results indicate an average delay of 197 ps with a standard deviation of 52 ps. The delay histogram is slightly skewed due to the lower limit on the flipping delay.

Fig. 10 illustrates dependency of θ_{i-rms} on temperature. As the temperature increases and approaches the Curie level, it is expected that the fluctuations increase since $H \rightarrow 0$ as temperature approaches T_C . By plotting the value of θ_{i-rms} between 200 K and 400 K in Fig. 10, it is observed that Nickel and Terfenol-D demonstrate more fluctuations mainly owing to their lower T_C values. The higher fluctuations will

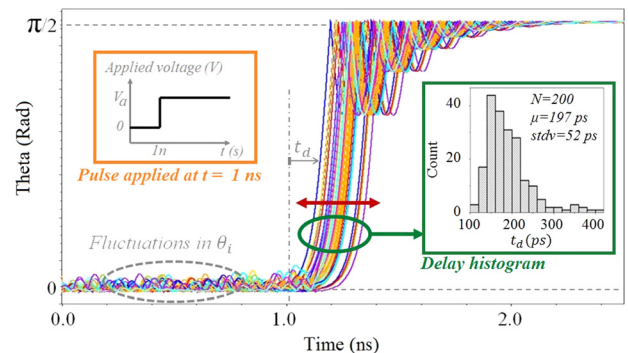


FIG. 9. Due to the random nature of the initial angle, the flipping delay varies with a skewed Gaussian distribution as demonstrated in the inset of the figure; at room temperature, the mean value of the delay is observed to be 197ps with merely 52ps of standard deviation; the left inset is the voltage pulse, applied at $t = 1$ ns, and the right inset shows the histogram of the delay values on 200 plotted dynamic waveforms.

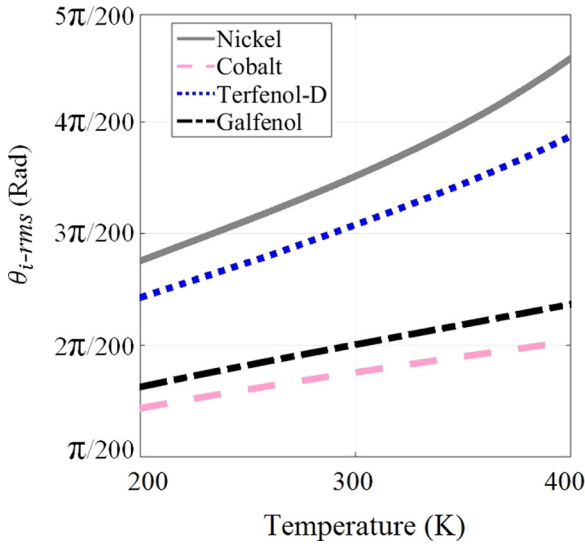


FIG. 10. The dependency of the initial magnetization angle on temperature; a higher temperature leads to more fluctuations due to the higher thermal noise.

assist with the easier flipping of the magnetization vector. Another parameter that can dramatically alter the value of θ_{i-rms} is the applied stress, as demonstrated in Fig. 11(a). As the stress levels reach their critical value for the four simulated materials, the initial angle approaches the value of $\pi/2$, owing to the stress-reduced energy barrier. From the basics of the straintronics principle, it is expected that when $\sigma > \sigma_C$, the magnetization settles along the minor axis, where $\theta = \pi/2$ and the magnetization vector will now fluctuate around this axis. The dynamic waveforms and histograms of the magnetization's fluctuations around the major axis along with their histograms at different stress levels below critical stress are also plotted in Fig. 11(b).

The dependency of the flipping delay on θ_{i-rms} is simulated and demonstrated in Fig. 12 for temperature ranges between 200 K and 400 K. As we increase the temperature, the value of θ_{i-rms} increases, leading to easier magnetization

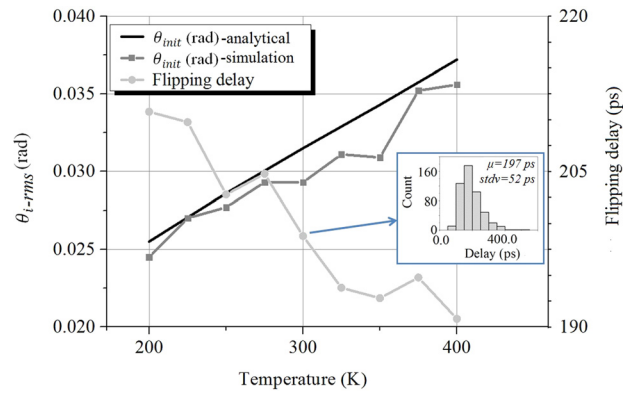


FIG. 12. Simulations results on Galfenol, showing the dependency of the initial angle and flipping delay on temperature along with the analytical data from (18); as temperature rises, the initial angle increases and the delay decreases slightly.

flipping and, therefore, a lower delay. The analytical data on the graph are the expected results from (18) and the simulated data are obtained from our Verilog-A model based on the thermally incorporated LLG dynamics in (15)–(17). The accuracy of the developed model can also be confirmed by comparing the analytical and simulated results.

The flipping delay of different materials, besides depending on the initial angle, is a strong function of the applied voltage (and therefore stress) across the straintronics device. In our previous work,¹⁵ we simulated different materials' flipping delay as a function of the applied voltage while assuming the same thermal noise for all the materials. Here, we analyzed the voltage dependency while including the materialy-dependent thermal noise. The four materials are simulated at room temperature and the results are recorded in Fig. 13, where it is observed that Terfenol-D has a very fast response owing to its high θ_{i-rms} (as expected from Fig. 10) and λ_s , while Cobalt shows a slow response due to its low θ_{i-rms} and λ_s . Nickel, although demonstrating a higher initial angle in Fig. 10, fails to compete with Galfenol and Terfenol-D due to its low λ_s . This confirms the

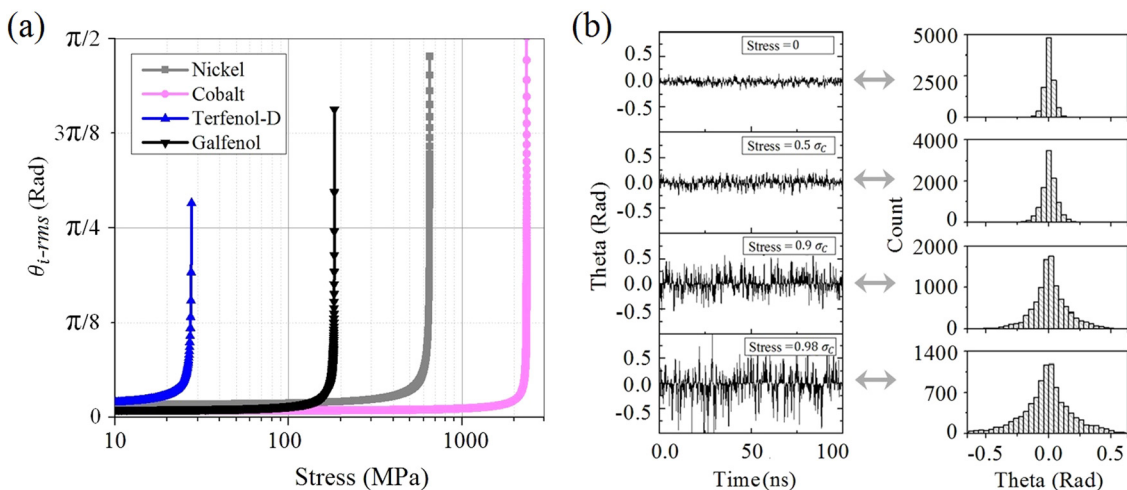


FIG. 11. (a) The dependency of the initial magnetization angle on the applied stress; as the stress approaches the critical values, the initial angle approaches $\pi/2$, as predicted by the stress anisotropy (b) dynamic waveforms and histograms of the initial angle of Galfenol for different stress levels, showing much larger fluctuations at high stress values.

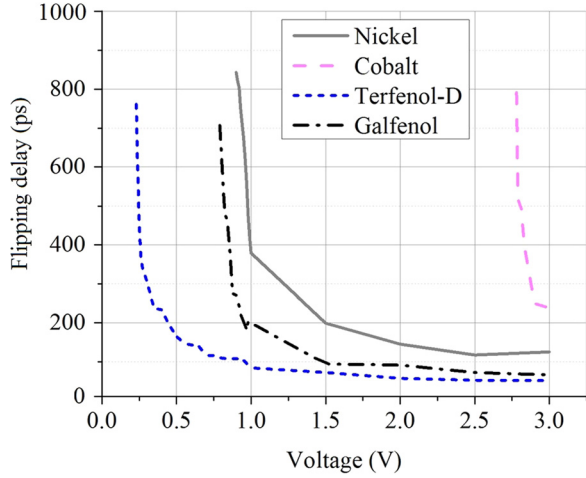


FIG. 13. Flipping delay for different magnetostrictive materials as a function of applied voltage's amplitude, showing the significant effect of high stress on flipping time of the nanomagnet.

suitability of Galfenol for integrated circuit applications due to its low critical flipping voltage, low flipping delay, and low variations of static features across temperatures between 200 K and 400 K as discussed earlier in Section III.

VI. TEMPERATURE DEPENDENCY OF DYNAMIC METRICS

In Section VII of this paper, some of the important metrics related to non-volatile memory design, an important application of straintronics devices, will be discussed. The effect of thermal noise and temperature variations on WEP and the speed-WEP trade-off will be analyzed. A write method that improves the energy and performance of the straintronics-based memories will be proposed. The effect of stress on the flipping delay and the HEP of the device will be analyzed in order to investigate the reliability and advantages of the proposed method.

A. Write error probability

One of the important obstacles in memory design is the probability of write error during the write operation, abbreviated as WEP. Consider any memory with a certain write pulsewidth, demonstrated in the inset of Fig. 14(a). The duration of the pulsewidth indicates the write speed of the memory. If a higher speed is desired, the pulsewidth can be

reduced. However, since the speed of writing in any memory cell is limited, there is a lower bound, beyond which the pulsewidth cannot be reduced. This lower bound is usually selected according to the memory's write error tolerance. For example, consider the straintronics device of Fig. 1(a). The application of a pulse with an amplitude higher than V_C will force the magnetization vector to settle along the minor axis ($\theta = \pi/2$) as demonstrated in Fig. 1(b). Due to the random nature of the Langevin thermal noise, the flipping delay can take a range of values as demonstrated in Fig. 14(a). Write error is associated with cases, where the delay is higher than the write pulsewidth, in which the magnetization vector will fail to flip.

Due to the Gaussian distribution of the flipping delay, demonstrated in Fig. 9, the WEP is expected to reduce significantly as we increase the write pulsewidth, which is demonstrated in Fig. 14(b). On the other hand, a longer pulsewidth is associated with a slower memory. Therefore, there is a trade-off between speed and WEP. As can be seen in the graphs, a reduced write speed from 0.2 ns to 0.4 ns leads to more than 1000X lower WEP at room temperature. In memory applications, the pulsewidth does not need to be increased further than the system's WEP requirements.

The effect of temperature on WEP can also be observed in Fig. 14(b), where we simulated Galfenol for different pulsewidths at different temperatures. A lower WEP at higher temperatures is mainly due to the increased θ_{i-rms} from 200 K to 400 K, as expected from (18).

B. A proposed write method, the energy-performance trade-off, and hold error probability

When it comes to memory design, energy and performance are two of the most important metrics. A considerable amount of research has been going on to reduce the write energy while retaining the speed of the MTJ-based memories.⁵⁷⁻⁶⁰

The switching energy, associated with the flipping of the straintronics device, can be formulated as¹⁶

$$E = C_{PZT}\Delta V^2 + E_d, \quad (19)$$

where C_{PZT} is the capacitance of the piezoelectric layer, ΔV is the voltage swing across the device, and E_d is the dissipated energy due to the Gilbert damping.⁶¹ For the devices with high energy barriers, the critical voltage is high enough

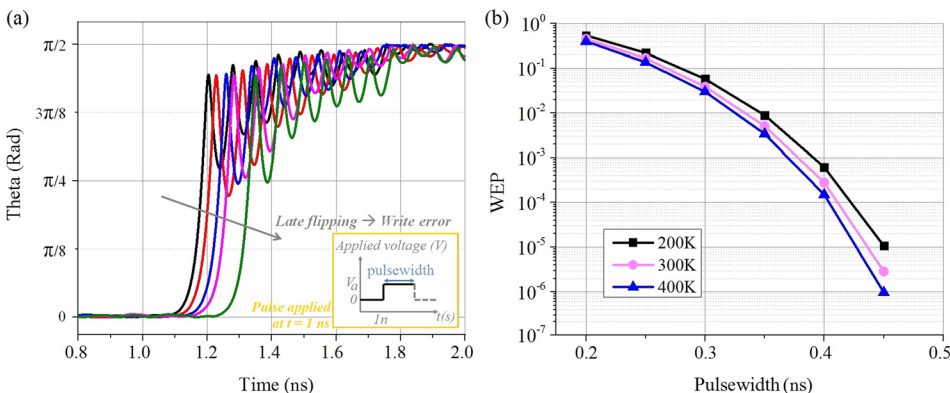


FIG. 14. Dynamic waveforms for Galfenol, demonstrating the possibility of write error due to late flipping; the inset of the figure shows the voltage pulse, applied at $t = 1$ ns, and (b) WEP as a function of pulsewidth and temperature; it is evident that as the pulsewidth is increased, the WEP decreases dramatically; increasing temperature will also reduce the WEP slightly for a given pulsewidth due to the dependency of the initial angle of temperature in (18).

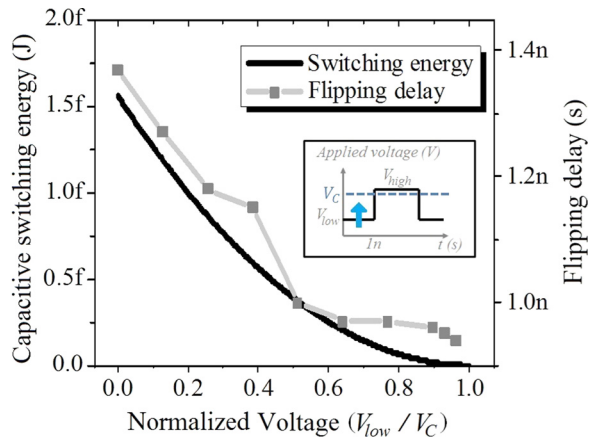


FIG. 15. By increasing the value of V_{low} closer to the critical voltage of Galfenol, the capacitive switching energy and flipping delay decrease.

to assure that the capacitive switching will consume the majority of the total switching energy. The switching energy can be significantly reduced if the voltage swing across the device is reduced, as demonstrated in the inset of Fig. 15. Increasing the value of V_{low} to the levels closer to V_C has two main advantages: (i) as $\Delta V = V_{high} - V_{low}$ reduces, the capacitive switching energy will drop as demonstrated for Galfenol in Fig. 15, where we fixed V_{high} slightly above V_C and started sweeping V_{low} from 0 to V_C . When $V_{low} \approx V_C$, the capacitive switching will consume negligible energy; (ii) the flipping delay will reduce as V_{low} increases as demonstrated in Fig. 15. The latter is expected since a higher V_{low} will create some stress across the device, reducing the energy barrier and increasing θ_{i-rms} according to (18). Therefore, a higher V_{low} leads to a higher θ_{i-rms} , which is associated with a faster flipping. This is further demonstrated in Fig. 16, where the delay histograms are plotted. The mean of the distributions moves towards smaller delays when the value of V_{low} is raised. Note that in the simulations of Figs. 15 and 16, V_{high} is set to be slightly higher than V_C . Should the value of V_{high} be increased, the delay will be reduced significantly, as already discussed in Section V.

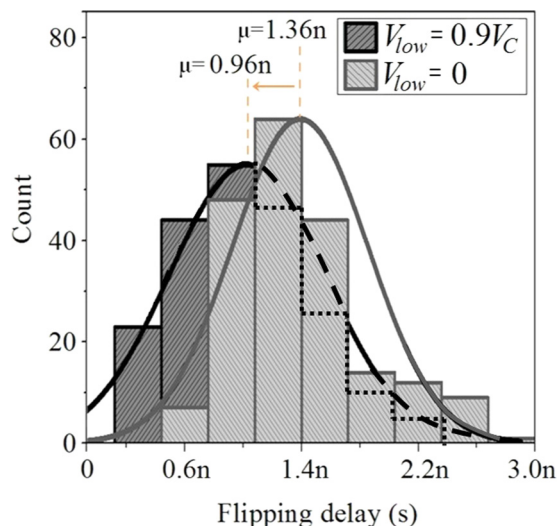


FIG. 16. Histograms of the flipping delays, demonstrating the reduction in the flipping delay due to higher V_{low} .

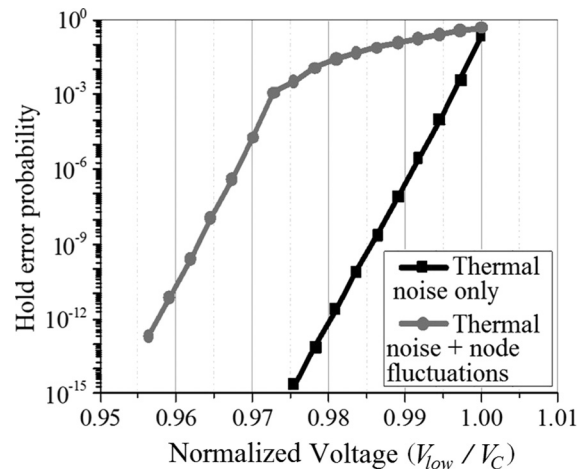


FIG. 17. HEP as a function of V_{low} in the presence of thermal noise only, and in the presence of both thermal noise and 1% voltage node fluctuations.

In order to analyze the reliability of the proposed method, we simulated the HEP of our straintronics device as an important data retention related property for non-volatile memories. It is expected that as we increase V_{low} , the HEP will reduce due to the increased thermal noise fluctuations. This phenomenon is demonstrated in Fig. 17, where we increased V_{low} to values close to V_C and plotted the resulting HEP of the device in two cases. First, we only assumed the presence of the Langevin thermal noise, and then we included 1% fluctuations of the applied V_{low} , which can frequently happen due to clock feedthrough in the ICs.⁶² In the first case, the HEP is negligible as long as V_{low} is kept below $0.97V_C$. In the second case, the HEP is noticeably higher compared to the first case, but reduces to negligible values as V_{low} goes below $0.95V_C$.

In the above simulations, the possibility of dimension changes due to process variations is not considered. Assuming that the effect of process variations on the device's dimensions is included, the value of V_{low} will decrease accordingly. In any event, from the above discussions, it can be concluded that reducing the voltage swing while retaining the value of V_{low} reliably below V_C will increase the energy efficiency and performance of the system while providing enough noise margin to keep the HEP well below the system's error tolerance. Nevertheless, it should be noted that the value of HEP is a strong function of the device's energy barrier. Should the energy barrier be decreased, the value of HEP in Fig. 17 will increase.

VII. CONCLUSION

A comprehensive study was performed on the effect of temperature on the magnetic properties of the straintronics device. The effect of temperature variations up to the Curie temperature on the energy barrier and the critical voltage of the device were analyzed. Four different magnetostrictive materials were simulated in order to provide a comprehensive platform for different applications. The effect of thermal noise was examined by incorporating the Langevin random field into the LLG equation and investigating the effect of temperature and stress on the initial magnetization angle.

Lastly, the effect of temperature and thermal noise on some of the important metrics for the nonvolatile memory design was studied and an energy efficient write method was introduced that can reliably reduce the capacitive switching energy and the flipping delay of the straintronics devices.

ACKNOWLEDGMENTS

This work was done partially under NSF NEB Grant No. ECCS-1124714 (PT106594-SC103006) and partially under AFOSR Grant No. FA9550-12-1-0402.

- ¹M. Julliere, *Phys. Lett. A* **54**, 225 (1975).
- ²D. Tang, P. Wang, V. Speriosu, S. Le, and K. Kung, *IEEE Trans. Magn.* **31**, 3206 (1995).
- ³T. Kenneth, D. Denny, and W. P. Kang, U.S. patent 5,343,422 (1994).
- ⁴Y. Zheng and J.-G. Zhu, *IEEE Trans. Magn.* **32**, 4237 (1996).
- ⁵J. Slonczewski, *J. Magn. Magn. Mater.* **159**, L1 (1996).
- ⁶R. Scheuerlein, in IEEE International Solid-State Circuits Conference (San Francisco, Feb 9, 2000).
- ⁷Z. Li and S. Zhang, *Phys. Rev. B* **68**, 024404 (2003).
- ⁸Y. Huai, F. Albert, P. Nguyen, M. Pakala, and T. Valet, *Appl. Phys. Lett.* **84**, 3118 (2004).
- ⁹Z. Zhu, G. Su, Q. Zheng, and B. Jin, *Phys. Rev. B* **68**, 224413 (2003).
- ¹⁰Z. Li and S. Zhang, *Phys. Rev. B* **69**, 134416 (2004).
- ¹¹K. Chun, H. Zhao, J. Harms, T. Kim, J. Wang, and C. Kim, *IEEE J. Solid-State Circuits* **48**, 598 (2013).
- ¹²J. Kim *et al.*, in IEEE 72nd Device Research Conference (Santa Barbara, June 22–25 2014)
- ¹³S. Salahuddin and S. Datta, *Appl. Phys. Lett.* **90**, 093503 (2007).
- ¹⁴N. Lei *et al.*, *Nat. Commun.* **4**, 1378 (2013).
- ¹⁵M. Barangi and P. Mazumder, *Appl. Phys. Lett.* **104**, 162403 (2014).
- ¹⁶K. Roy, S. Bandyopadhyay, and J. Atulasimha, *Appl. Phys. Lett.* **99**, 063108 (2011).
- ¹⁷A. Khan, D. Nikonov, S. Manipatruni, T. Ghani, and I. Young, *Appl. Phys. Lett.* **104**, 262407 (2014).
- ¹⁸S. Kim, S. Shin, and K. No, *IEEE Trans. Magn.* **40**, 2637 (2004).
- ¹⁹S. Chikazumi, C. Graham, and S. Chikazumi, *Physics of Ferromagnetism* (Oxford University Press, Oxford, 1997).
- ²⁰J. Alzate, P. Khalili Amiri, G. Yu, P. Upadhyaya, J. Katine, J. Langer, B. Ocker, I. Krivorotov, and K. Wang, *Appl. Phys. Lett.* **104**, 112410 (2014).
- ²¹J. Restorff and M. Wun-Fogle, *J. Appl. Phys.* **107**, 09A913 (2010).
- ²²Y. Ming-Hui and Z. Zhi-Dong, *Phys. Rev. B* **60**, 12107 (1999).
- ²³Y. Wang and V. Chodavarapu, *Sensors* **15**, 4253 (2015).
- ²⁴S. Giordano, Y. Dusch, N. Tiercelin, P. Pernod, and V. Preobrazhensky, *Eur. Phys. J. B* **86**, 249 (2013).
- ²⁵S. Giordano, Y. Dusch, N. Tiercelin, P. Pernod, and V. Preobrazhensky, *J. Phys. D: Appl. Phys.* **46**, 325002 (2013).
- ²⁶A. Biswas, S. Bandyopadhyay, and J. Atulasimha, *Appl. Phys. Lett.* **104**, 232403 (2014).
- ²⁷K. Munira, Y. Xie, S. Nadri, M. Forgues, M. Fashami, J. Atulasimha, S. Bandyopadhyay, and A. Ghosh, *Nanotechnology* **26**, 245202 (2015).
- ²⁸M. Barangi and P. Mazumder, *IEEE Trans. Magn.* **51**, 1–8 (2015).
- ²⁹M. Barangi and P. Mazumder, *IEEE Nanotechnol. Mag.* **9**, 15–24 (2015).
- ³⁰M. Barangi and P. Mazumder, in International Conference on Simulation of Semiconductor Process and Devices (SISPAD) (Washington D.C., September 9–11, 2015).
- ³¹See supplementary material at <http://dx.doi.org/10.1063/1.4934566> for the detailed analysis on saturation magnetization and the dynamic thermal noise.
- ³²E. Callen and H. Callen, *Phys. Rev.* **129**, 578 (1963).
- ³³R. Skomski, O. Mryasov, J. Zhou, and D. Sellmyer, *J. Appl. Phys.* **99**, 08E916 (2006).
- ³⁴A. E. Clark, M. Wun-Fogle, J. B. Restorff, and T. A. Lograsso, *Mater. Trans.* **43**, 881 (2002).
- ³⁵C. Paduani and C. Bormio-Nunes, *J. Appl. Phys.* **109**, 033705 (2011).
- ³⁶D. Laughlin, K. Srinivasan, M. Tanase, and L. Wang, *Scr. Mater.* **53**, 383 (2005).
- ³⁷O. Mryasov, U. Nowak, K. Guslienko, and R. Chantrell, *Europhys. Lett.* **69**, 805 (2005).
- ³⁸R. Skomski, *J. Appl. Phys.* **83**, 6503 (1998).
- ³⁹K. Sato, Y. Isikawa, K. Mori, A. Clark, and E. Callen, *J. Magn. Magn. Mater.* **54–57**, 875 (1986).
- ⁴⁰K. Prajapati, A. Jenner, and R. Greenough, *IEEE Trans. Magn.* **31**, 3976 (1995).
- ⁴¹R. Bergstrom, Jr., Ph.D. thesis, University of Maryland, 2013.
- ⁴²J. Restorff, M. Wun-Fogle, A. Clark, and K. Hathaway, *IEEE Trans. Magn.* **42**, 3087 (2006).
- ⁴³S. Lim, S. Kim, S. Kang, J. Park, J. Nam, and D. Son, *J. Magn. Magn. Mater.* **191**, 113 (1999).
- ⁴⁴J. Kouvel and M. Fisher, *Phys. Rev.* **136**, A1626 (1964).
- ⁴⁵R. V. Colvin and S. Aarj, *J. Phys. Chem. Solids* **26**, 435 (1965).
- ⁴⁶N. Cordente *et al.*, *Nano Lett.* **1**, 565 (2001).
- ⁴⁷Terfenol-D datasheet, (c) 2015 Etrema Products Ins., www.etrema.com/terfenol-d/.
- ⁴⁸M. Chaudhri, W. Corner, and A. Joraide, *J. Magn. Magn. Mater.* **65**, 53 (1987).
- ⁴⁹E. Callen and H. Callen, *Phys. Rev.* **139**, A455 (1965).
- ⁵⁰A. Clark, J. Teter, and O. McMasters, *J. Appl. Phys.* **63**, 3910 (1988).
- ⁵¹D. Bower, *Proc. R. Soc. A* **326**, 87 (1971).
- ⁵²C. W. Smullen *et al.*, in IEEE 17th International Symposium on High Performance Computer Architecture (San Antonio, TX, Feb. 12–16, 2011).
- ⁵³F. G. Sanchez, Ph.D. dissertation, Universidad Autonoma de Madrid, 2007.
- ⁵⁴W. Brown, *Phys. Rev.* **130**, 1677 (1963).
- ⁵⁵G. Grinstein and R. Koch, *Phys. Rev. Lett.* **90**, 207201 (2003).
- ⁵⁶S. Manipatruni, D. Nikonov, and I. Young, *IEEE Trans. Circuits Syst. I* **59**, 2801 (2012).
- ⁵⁷R. Heindl, W. Rippard, S. Russek, and A. Kos, *Phys. Rev. B* **83**, 054430 (2011).
- ⁵⁸Z. Sun, X. Bi, H. Li, W. Wong, and X. Zhu, *IEEE Trans. VLSI Syst.* **22**, 1281 (2014).
- ⁵⁹W. Wang, M. Li, S. Hageman, and C. Chien, *Nature Mater.* **11**, 64 (2011).
- ⁶⁰W. Wen, Y. Zhang, Y. Chen, Y. Wang, and Y. Xie, *IEEE Trans. Comput.-Aided Des. Integr. Circuits Syst.* **33**, 1644 (2014).
- ⁶¹B. Behin-Aein *et al.*, *IEEE Trans. Nanotechnol.* **8**, 505 (2009).
- ⁶²J. Rabaey, A. Chandrakasan, and B. Nikolic, *Digital Integrated Circuits* (Pearson Education, Upper Saddle River, NJ, 2003).